Effects of a Delocalizable Cation on the Headgroup of Gemini Lipids on the Lipoplex−Type Nanoaggregates Directly Formed from Plasmid DNA

ARTICLE *in* BIOMACROMOLECULES · OCTOBER 2013

Impact Factor: 5.75 · DOI: 10.1021/bm401079h · Source: PubMed

10 AUTHORS, INCLUDING:

Mónica Muñoz Ubeda
Materials Science Institute of Barcelona
12 PUBLICATIONS **202** CITATIONS
SEE PROFILE

Sougata Datta
Indian Institute of Science
15 PUBLICATIONS **149** CITATIONS
SEE PROFILE

Ana Lilia Barrán Berdón
Complutense University of Madrid
12 PUBLICATIONS **177** CITATIONS
SEE PROFILE

Pablo Castro Hartmann
Autonomous University of Barcelona
17 PUBLICATIONS **102** CITATIONS
SEE PROFILE

Article

pubs.acs.org/Biomac

Effects of a Delocalizable Cation on the Headgroup of Gemini Lipids on the Lipoplex-Type Nanoaggregates Directly Formed from Plasmid DNA

Santosh K. Misra,[†,‡] Mónica Muñoz-Úbeda,[†,§] Sougata Datta,[‡] Ana L. Barrán-Berdón,[§] Clara Aicart-Ramos,[∥] Pablo Castro-Hartmann,[⊥] Paturu Kondaiah,[⊥] Elena Junquera,[§] Santanu Bhattacharya,*[,‡] and Emilio Aicart*[,§]

Departments of [‡]Organic Chemistry and [⊥]Molecular Reproduction Development and Genetics, Indian Institute of Science, 560012 Bangalore, India

[§]Grupo de Química Coloidal y Supramolecular, Departamento de Química Física I, and [∥]Departamento de Bioquímica y Biología Molecular I, Facultad de Ciencias Químicas, Universidad Complutense de Madrid, 28040 Madrid, Spain

[⊥]Servei de Microscopia, Universitat Autónoma de Barcelona, 08193 Cerdanyola del Vallés, Spain

Supporting Information

ABSTRACT: Lipoplex-type nanoaggregates prepared from pEGFP-C3 plasmid DNA (pDNA) and mixed liposomes, with a gemini cationic lipid (CL) [1,2-bis(hexadecyl imidazolium) alkanes], referred as $(C_{16}Im)_2C_n$ (where C_n is the alkane spacer length, n = 2, 3, 5, or 12, between the imidazolium heads) and DOPE zwitterionic lipid, have been analyzed by zeta potential, gel electrophoresis, SAXS, cryo-TEM, fluorescence anisotropy, transfection efficiency, fluorescence confocal microscopy, and cell viability/cytotoxicity experiments to establish a structure−biological activity relationship. The study, carried out at several mixed liposome compositions, α, and effective charge ratios, ρ_{eff}, of the lipoplex, demonstrates that the transfection of pDNA using CLs initially requires the determination of the effective charge of both. The electrochemical study confirms that CLs with a delocalizable positive charge in their headgroups yield an effective positive charge that is 90% of their expected nominal one, while pDNA is compacted yielding an effective negative charge which is only 10−25% than that of the linear DNA. SAXS diffractograms show that lipoplexes formed by CLs with shorter spacer (n = 2, 3, or 5) present three lamellar structures, two of them in coexistence, while those formed by CL with longest spacer (n = 12) present two additional inverted hexagonal structures. Cryo-TEM micrographs show nanoaggregates with two multilamellar structures, a cluster-type (at low α value) and a fingerprint-type, that coexist with the cluster-type at moderate α composition. The optimized transfection efficiency (TE) of pDNA, in HEK293T, HeLa, and H1299 cells was higher using lipoplexes containing gemini CLs with shorter spacers at low α value. Each lipid formulation did not show any significant levels of toxicity, the reported lipoplexes being adequate DNA vectors for gene therapy and considerably better than both Lipofectamine 2000 and CLs of the 1,2-bis(hexadecyl ammnoniun) alkane series, recently reported.

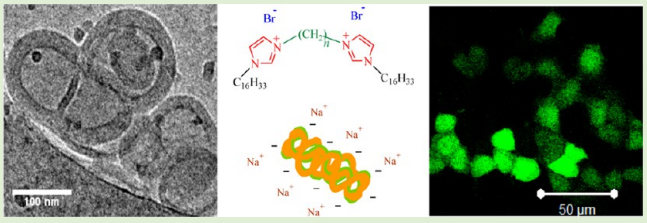

INTRODUCTION

Gene therapy employs "Gene as medicine" in modern medical research.[1] In the early phase of this research area, natural viruses were used as gene transporters.[2] However, due to their extremely adverse immune reactivity toward the therapeutic applications, attraction has been shifted to the design and syntheses of nonviral gene transfection agents, such as cationic lipids (CLs) that form lipoplexes with DNA. For the success of such a nonviral gene transfection strategy, the biophysical nature of the lipoplex should be studied thoroughly in relation to the viral gene transfection agents. DNA is a biopolymer that in aqueous solution remains negatively charged and adopts a conformation dependent on its topology. Due to this, electrostatic interactions play an important role in any of the biological processes where the delivery of gene is involved. The use of synthetic CLs as transfection agents for nucleic acids in gene therapy has been the subject of many studies.[3−20] Among the wide variety of CLs, those known as gemini CLs are raising a remarkable interest due to their lower toxicity, compared with that of the monomeric CLs. The complexation process is based on the compaction of DNA by a CL, usually mixed with an additional helper lipid, with the formation of a lipoplex, with a net positive charge between the cationic mixed liposome and the anionic plasmid DNA. A strong interaction between both components of the nanoaggregate (mixed lipid-DNA) permits its adherence to the cell membranes, the DNA being liberated

Received: July 23, 2013
Revised: September 20, 2013
Published: October 1, 2013

Scheme 1. Molecular Structure of (a) Gemini Cationic Lipids [1,2-Bis(hexadecyl imidazol) Alkane], $(C_{16}Im)_2C_n$, where n = 2, 3, 5, or 12, and (b) Zwitterionic Helper Lipid, 1,2-Dioleoyl-*sn*-glycero-3-phosphatidylethanolamine (DOPE)

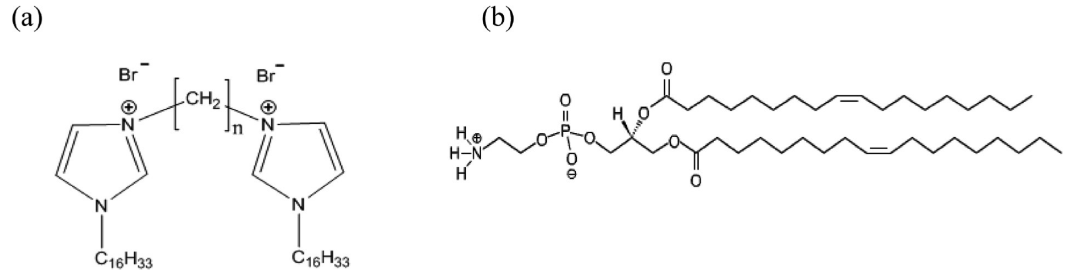

in the cytoplasm via the nucleus of the cell, after fusion or endocytosis.[21] Thus, a biophysical study of the compaction process of DNA by CLs, based on both electrochemical and structural characterization, may help in understanding better the behavior of the lipoplex nanoaggregates and the mechanisms of the DNA transfection process. Previous investigations,[19,21−27] which analyzed different kinds of lipoplexes, have found a correlation between their structure (lamellar or hexagonal) and the type and composition of the mixed lipid used in the DNA compaction. The TE of the DNA was found to be strongly related with those nanostructures. For these reasons, it is important to carry out precise physicochemical studies with lipoplexes formed from new cationic lipids in search of more efficient vectors for gene therapy.

Furthermore, we have recently demonstrated[19,20,28] that it is absolutely necessary to consider both the effective CL positive charge, $q^+_{L^+}$, and the effective pDNA negative charge, q^-_{pDNA}. These must be determined from physicochemical experiments, before choosing the appropriate effective charge ratios, ρ_{eff}, between the CL and pDNA charges to carry out the biological experiments.

Localized positive charge based cationic lipids have been extensively investigated as gene delivery agents, but headgroups with delocalized positive charge are still not well studied. In literature, CLs containing imidazolium polar heads[29−31] have been reported to display higher transfection efficiency and reduced cytotoxicity when compared with classical quaternary ammonium cationic lipids.[32] Similarly, the incorporation of an imidazolium headgroup in phosphoramidate lipids resulted in a ∼100-fold improvement in the transfection efficiency comparable to a guanidinium counterpart of the compound, which induced very high cytotoxicity, suggesting that the imidazolium group is less harmful for the cells than the guanidinium.[33] The cytotoxic effect of CLs is associated with the cationic nature of the vectors. A recent solution to circumvent this problem was to spread the positive charge of the cationic head by delocalizing it into a heterocyclic ring.[34] Solodin and coworkers[35] revealed that, as compared with classical transfection systems, heterocyclic cationic lipids containing imidazolium polar heads possess both higher transfection efficiency and reduced cytotoxicity. Thus, yet not fully explored an imidazolium group might be worth considering for the design of new cationic lipids for nonviral gene delivery and establishing a quantitative correlation among their chemistry, morphology, structure and transfection efficiency.

In this work, and looking for improved gene vectors of plasmid DNA, we report a biophysical and biological study of lipoplex-type nanoagregates formed by four novel CLs of the series of gemini cationic lipids 1,2-bis(hexadecyl imidazolium) alkanes, referred to as $(C_{16}Im)_2C_n$, with n = 2, 3, 5, or 12, the neutral helper lipid 1,2-dioleoyl-*sn*-glycero-3-phosphatidylethanolamine (DOPE), and a supercoiled pEGFP-C3 plasmid DNA (pDNA) amplified and purified by us. DOPE is chosen since it is a fusogenic lipid that also decreases the cytotoxicity of the cationic lipids.[36−45] The $(C_{16}Im)_2C_n$ lipids are gemini cationic lipids synthesized by us that include two delocalizable cationic imidazolium units in their heads (see Scheme 1). They are expected to be less toxic and better pDNA tranfecting agents to cells than commercial formulations. The study has been performed from an analysis carried out by using a wide variety of experimental methods. First, electrochemical methods as zeta potential and gel electrophoresis have permitted the determination of effective charges of the cationic lipid, $q^+_{L^+}$, and of the plasmid DNA, q^-_{pDNA}, the electroneutrality ratio, $(L/D)_\phi$, where the positive charges of the CL and the negative ones of the pDNA balance (ρ_{eff} = 1), each other and the effective charge ratios between a particular CL and pDNA, ρ_{eff}, are obtained. We have employed cryogenic transmission electron microscopy (cryo-TEM), or small-angle X-ray scattering (SAXS), which provide information about the structure, size and morphology of those structures formed by pDNA and the mixed gemini cationic lipids/DOPE in the entire cationic lipid composition, α, of the lipid mixtures. We have also used fluorescence anisotropy, directly related with the fluidity of the bilayers of liposomes and lipoplexes, and biological methods such as flow cytometry, cell viability/cytotoxicity, and confocal fluorescence microscopy for the evaluation of the transfection efficiency (TE) and the cell viability of the plasmid DNA vectors proposed in this work. The findings of this study is expected to provide an understanding as to how a plasmid DNA is compacted and transfected to cells by improved mixed colloidal nanostructures that contain more biocompatible gemini cationic lipids with delocalizable positive charges in their headgroups.

■ EXPERIMENTAL SECTION

Materials. The divalent cationic gemini surfactants 1,2-bis-(hexadecyl imidazolium) alkanes referred to as $(C_{16}Im)_2C_n$, with the spacer n = 2, 3, 5, or 12, were synthesized according to a reported procedure[46] detailed in the Supporting Information (SI). All the compounds were characterized by ^1H NMR spectroscopy, mass spectrometry, and elemental analysis. Chemical shifts, δ, reported in ppm downfield from the internal standard (TMS) and the pertinent details are given in the SI. The zwitterionic lipid, 1, 2-dioleoyl-*sn*-glycero-3-phosphatidylethanolamine (DOPE) was used as received from Avanti Polar Lipids. Sodium salt of calf thymus DNA (ctDNA), provided by Sigma-Aldrich, was used as linear DNA to determine the lipid charge, $q^+_{L^+}$, of the cationic gemini surfactants. Large amounts (mg) of purified plasmid DNA was prepared using the GenElute HP Select Plasmid Gigaprep Kit (Sigma-Aldrich). Competent *E. coli*

DH5α cells were transformed with the pEGFP-C3 plasmid DNA (pDNA). Details of the procedure are reported in the SI. The recovered pDNA (4700 bp) was predominantly in its supercoiled conformation, as determined from ethidium bromide-stained agarose gel electrophoresis.

Preparation of Lipid Mixtures and Lipoplex Nanoaggregates. Appropriate amounts of gemini surfactant, L^+, and DOPE, L^0, were dissolved in chloroform to obtain the desired CL composition, α, of the mixed lipids (thus, $L = L^+ + L^0$, is the total mass of lipid). After brief vortexing, the solvent was evaporated under high vacuum to yield a dry lipid film that was finally hydrated with HEPES buffer, pH = 7.4. A combination of vortexing, sonication, and warming yields MLVs, which were transformed into the unilamellar liposomes, LUVs, by a sequential extrusion procedure, as explained elsewhere.[47] The pDNA concentrations (in mM base pairs) were obtained from the absorbance at 260 nm.[48,49] To obtain the desired lipoplex composition (in terms of the mass ratio, L/D, between total lipid, L, to plasmid DNA, D, or the effective charge ratio, ρ_{eff}, between the CL and pDNA charges, equal volumes of pDNA and $(C_{16}Im)_2C_n$/DOPE liposomal suspensions were mixed by adding pDNA over the mixed liposome solution (see SI for details of the procedure).

Zeta Potential. Electrophoretic mobilities were determined using a phase analysis light scattering technique (Zeta PALS, Brookhaven Instrum. Corp., U.S.A.) and from it zeta potential, ζ, was obtained (see SI).[19,28] Zeta potential values for the liposome and lipoplex-type nanoaggregates solutions were measured, at each CL composition, α, of the mixed liposome, as a function of the mass ratio of lipoplex composition, L/D.

Gel Electrophoresis. Lipoplex nanoaggregates along with uncomplexed, pure plasmid DNA were loaded on to 1% agarose gel and run at 100 mV in 1× TAE (Tris-HCl, acetate, and EDTA) buffer for ∼30 min. Gels were photographed under UV light. The amount of mixed liposome required to produce electrically neutral lipoplex was termed as pDNA binding efficiency of the mixed liposome. Fluorescence intensity of each band was measured using commercial Alfa-digi-Doc software provided with Gel-Doc instrument (see SI for additional details).

Small-Angle X-ray Scattering. SAXS experiments were carried out on the beamline 26 at European Synchrotron Radiation Facility (ESRF) Grenoble (France). The scattered X-ray was detected on MARCCD 165, converted to one-dimensional scattering by radial averaging, and represented as a function of the momentum transfer vector, q (see SI for additional information). SAXS experiments were run at different cationic lipid compositions, α, of the mixed lipid, and at several effective charge ratios, ρ_{eff}, of the lipoplex nanoaggregates.

Cryo-TEM. Experiments were prepared following the procedure described elsewhere[50,51] (see more details in the SI). Images were obtained using a Jeol JEM 2011 cryo-electron microscope operated at 200 kV and using different degrees of defocus to obtain an adequate phase contrast.[52] Images were recorded on a Gatan 794 Multiscan digital camera and processed and analyzed with a Digital Micrograph. Selected sections were plotted with the Profile tool to obtain histograms of gray level versus distance.

Fluorescence Anisotropy. Fluorescence anisotropy of 1,6-diphenylhexatriene (DPH) probe was measured with a Perkin-Elmer LS-50B Luminiscence Spectrometer following a protocol explained elsewhere[53] (more details can be found in the SI).

Transfection of pDNA. Transfection of pEGFP-C3 plasmid DNA across HEK293T (human embryo kidney transformed cancer), HeLa (human cervical cell carcinoma), H460 (human lung cancer), H1299 (nonsmall lung carcinoma), A549 (human alveolar basal epithilial), and NIH3T3 (mouse embryo fibroblast) cells using lipid mixtures $(C_{16}Im)_2C_n$/DOPE was performed in absence (-FBS-FBS) and presence (-FBS+FBS) of serum (see SI for details of the procedure). Harvested cells were used for the flow assisted cell sorting (FACS), and the number of cells with higher green fluorescence (% GFP cells), as well as the average intensity of fluorescence per cell (mean fluorescence intensity (MFI)), were obtained. Results were plotted as % GFP cells and MFI against effective charge ratio, ρ_{eff}, on Graph pad prism 5.0 software. Lipofectamine2000 was used as a positive control during all the transfection experiments.

Confocal Fluorescence Microscopy (CFM). CFM study was performed on cells transfected with pDNA, in the same way as in the transfection experiments. Working stocks of the lipoplexes were prepared in DMEM with (-FBS+FBS) and without (-FBS-FBS) serum. Control experiments were performed using commercial transfection reagent, Lipofectamine2000. The permeabilized monolayers of HEK293T cells were incubated with propidium iodide (PI) to specifically stain the nucleus of the cells (details of the procedure can be found in the SI). Samples were finally observed under a confocal microscope (Zeiss LSM 510-Meta Apochromat).

Cell Viability. The cell viability of each lipid formulation toward HEK293T cells was determined by using 3-(4,5-dimethylthiazole-2-yl)-2,5-diphenyl tetrazolium bromide reduction method (MTT assay) following a procedure already reported in the literature,[54,55] as well as in the SI. Lipoplexes, prepared at various effective charge ratios, ρ_{eff}, were incubated with cells for 6, 24, and 48 h. Finally, MTT were added to each well, and after incubating the mixtures, blue formazan crystals were seen under microscope. The absorbance was measured using a microtiter plate reader. As reported in the SI, the % cell viability was then calculated from readings obtained from ELISA reader.

RESULTS AND DISCUSSION

Effective Charges of the Cationic Lipid and the Plasmid DNA and Electroneutrality of the Lipoplex Nanoaggregates. The composition of the mixed liposome and the effective charge ratio of the lipoplex are known to be determinant in the behavior, characteristics, structures and potential performances of lipoplexes as gene vectors. Liposome composition is usually given as the CL molar fraction, α, while either the total lipid to DNA mass ratio, L/D, or the effective charge ratio, ρ_{eff}, between the charge of positive CL and negative DNA phosphate groups are used to define the composition of the lipoplex. These quantities are related by the following equations:

$$\alpha = \frac{L^+/M_{L^+}}{(L^+/M_{L^+}) + (L^0/M_{L^0})} \quad (1)$$

$$\rho_{eff} = \frac{n^+}{n^-} = \frac{q^+_{L^+}L^+/M_{L^+}}{q^-_{DNA}D/\bar{M}_{bp}} \quad (2)$$

where M_{L^+} and M_{L^0} are the molar masses of cationic and helper lipids; n^+ and n^- are the number of moles of positive and negative charges, coming from CL and DNA; $q^+_{L^+}$ and q^-_{DNA} are the charges of CL and DNA base pair; and $\bar{M}_{bp}$ is the average molar mass per DNA base pair. Because efficient cell transfection requires net positive lipoplex nanoaggregates capable of going through the negatively charged cell membrane, there is one particular L/D value, called electroneutrality ratio, $(L/D)_\phi$, where the positive and negative charges balance ($\rho_{eff} = 1$); this ratio marks the lower limit from which the nanoaggregate becomes a potentially efficient cell transfecting agent.[8,56]

Because zeta potential is related to the net charge of the nanoaggregates, it reveals as the best physicochemical property to provide this information, although ethidium bromide or GelRed intercalation assays, or agarose gel electrophoresis could also be used. Figures 1a and S-1 of the Supporting Information (SI) show plots of zeta potential, ζ, versus L/D, at $\alpha = 0.5$, for the four CLs used in this work. The electroneutrality ratio $(L/D)_\phi$ of the nanoaggregate can be determined as the L/D where a sign inversion on the charge

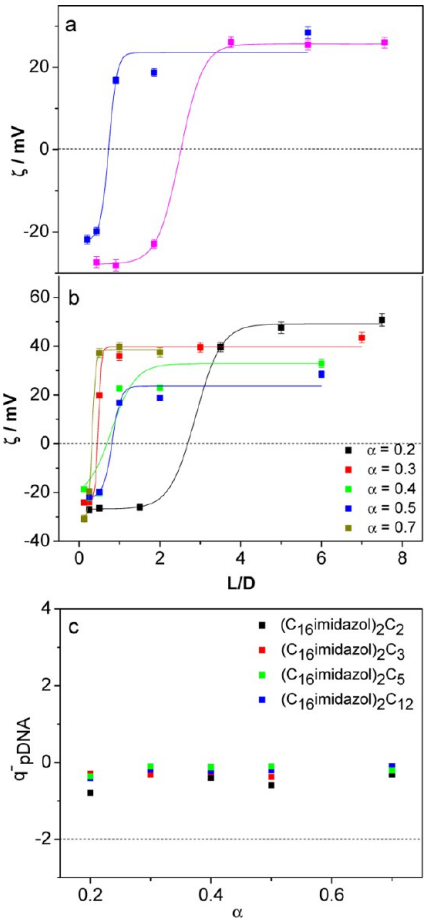

Figure 1. Plots of zeta potential, ζ, against the lipoplex nanoaggregate composition (L/D) of (a) $(C_{16}Im)_2C_2$/DOPE-pDNA (blue) and $(C_{16}Im)_2C_2$/DOPE-ctDNA (pink), at CL composition, α = 0.5; and (b) $(C_{16}Im)_2C_2$/DOPE-pDNA at different CL composition, α. Solid line: sigmoidal fit of experimental values. Errors are within ±5%. Effective pDNA charge for $(C_{16}Im)_2C_n$/DOPE-pDNA (n = 2, 3, 5, or 12) lipoplexes vs CL composition, α, are shown in (c).

occurs on the ζ sigmoidal profiles. This value is related with the previous quantities by

$$\left(\frac{L}{D}\right)_{\phi} = \frac{q^-_{DNA}[\alpha M_{L^+} + (1-\alpha)M_{L^0}]}{q^+_{L^+}\alpha \bar{M}_{bp}} \quad (3)$$

Extensive studies reported in literature have shown that linear DNA, as calf thymus DNA, salmon sperm DNA, or so on, has its negative charge totally available for the cationic lipid, that is, $q^-_{linearDNA} = -2$ per bp. But experiments reported by us recently,[19,20,28] have demonstrated that, at physiological pH and depending on the ionic strength, plasmid DNA remains in a supercoiled conformation[57,58] that renders a considerably less negative charge than its nominal one, that is, $q^-_{pDNA} \ll -2$. For that reason, any biophysical or biological study about lipoplexes must start with the determination of the real or effective charge of both the cationic lipid, $q^+_{L^+}$, and the plasmid DNA, q^-_{pDNA}, when forming the lipoplex.

Thus, in a first step, the effective charge of the CL, $q^+_{L^+}$, can be determined for a certain CL composition, α, of the mixed liposome, using eq 3 and the $(L/D)_{\phi}$ value of the CL/DOPE-linear DNA lipoplex experimentally measured from zeta potential, and assuming $q^-_{linearDNA} = -2$. The $q^+_{L^+}$ values thus obtained (see Table S-1) are usually close to its expected nominal charge (+2 for a gemini type CL with two cationic heads). Table 1 reports $q^+_{L^+}$ results for the four gemini CLs of this work, the average value being $q^+_{L^+} = (1.7 \pm 0.1)$ for the $(C_{16}Im)_2C_n$ series with n = 2, 3, 5, or 12. Once $q^+_{L^+}$ is known, the second step is focused on the determination of $(L/D)_{\phi}$ for the lipoplex, but now containing plasmid DNA in identical mixed lipid composition, α, that is, the CL/DOPE-pDNA lipoplex (see Figures 1b and S-2 and Table S-1 of SI). Afterward, the effective charge of the plasmid DNA, q^-_{pDNA}, can be obtained using eq 4 after rearranging the eq 3:

Table 1. Values of the Cationic Lipid Charge, $q^+_{L^+}$, and the Effective pDNA Charge, q^-_{pDNA}, for $(C_{16}Im)_2C_n$/DOPE-pDNA, Experimentally Obtained from Zeta Potential for the Four Series (with n = 2, 3, 5, or 12) Studied in this Work

n	$q^+_{L^+}$	q^-_{pDNA}
2	1.7	−0.46
3	1.6	−0.23
5	1.8	−0.18
12	1.7	−0.19

$$q^-_{pDNA} = \left(\frac{L}{D}\right)_{\phi}\left(\frac{q^+_{L^+}\alpha \bar{M}_{bp}}{[\alpha M_{L^+} + (1-\alpha)M_{L^0}]}\right) \quad (4)$$

The q^-_{pDNA} results at various CL compositions, α, for the four CL/DOPE-pDNA lipoplexes of this work are plotted in Figure 1c. The effective charge of pDNA, q^-_{pDNA}, have been also obtained from gel electrophoresis experiments (Figure S-3), the values thus obtained being in very good agreement with the zeta potential results. In general, the q^-_{pDNA} values are roughly constant with α, but for a given α, the average values (absolute values) reported in Table 1 show a slight decrease with the spacer length of the gemini CL. In any case, the values of q^-_{pDNA} obtained in this work, together with those previously reported,[19,20,28] confirm that plasmid DNA renders an effective negative charge lower than its nominal one, when forms nanoaggregates with CLs. As the lipoplex nanoaggregate must be positive to adhere to cell membrane, q^-_{pDNA} values that are ~10−25% (in absolute value) of the expected ones (if q^-_{DNA} was −2) imply that less amount of CL is required to prepare appropriate lipoplexes for carrying out an effective transfection, which, in turn, has an advantageous effect of decreasing the cytotoxicity.

Once the real charges of cationic lipid, $q^+_{L^+}$, and of pDNA, q^-_{pDNA}, are correctly obtained, the effective charge ratio, ρ_{eff}, between the CL positive charges and the negative ones coming from DNA phosphate groups, may be also calculated by substituting $q^+_{L^+}$ and q^-_{pDNA} in eq 2. The ρ_{eff} quantity is the key to prepare lipoplex nanoaggregates with optimum performances toward transfection, that is, with a net positive charge and with the lowest level of cytotoxicity.

Structure, Morphology and Bilayer Fluidity of the Lipoplex Nanoaggregates. Structure, size, and morphology of the $(C_{16}Im)_2C_n$/DOPE-pDNA lipoplexes have been analyzed by means of SAXS and cryo-TEM experiments. First, the size of the mixed liposomes was determined with the PALS technique. The average hydrodynamic diameters of (92 ± 15), (95 ± 10), (95 ± 8), and (93 ± 6) nm, obtained for the $(C_{16}Im)_2C_n$/DOPE mixed liposomes where n = 2, 3, 5, or 12, respectively, are consistent with the extrusion protocol[47]

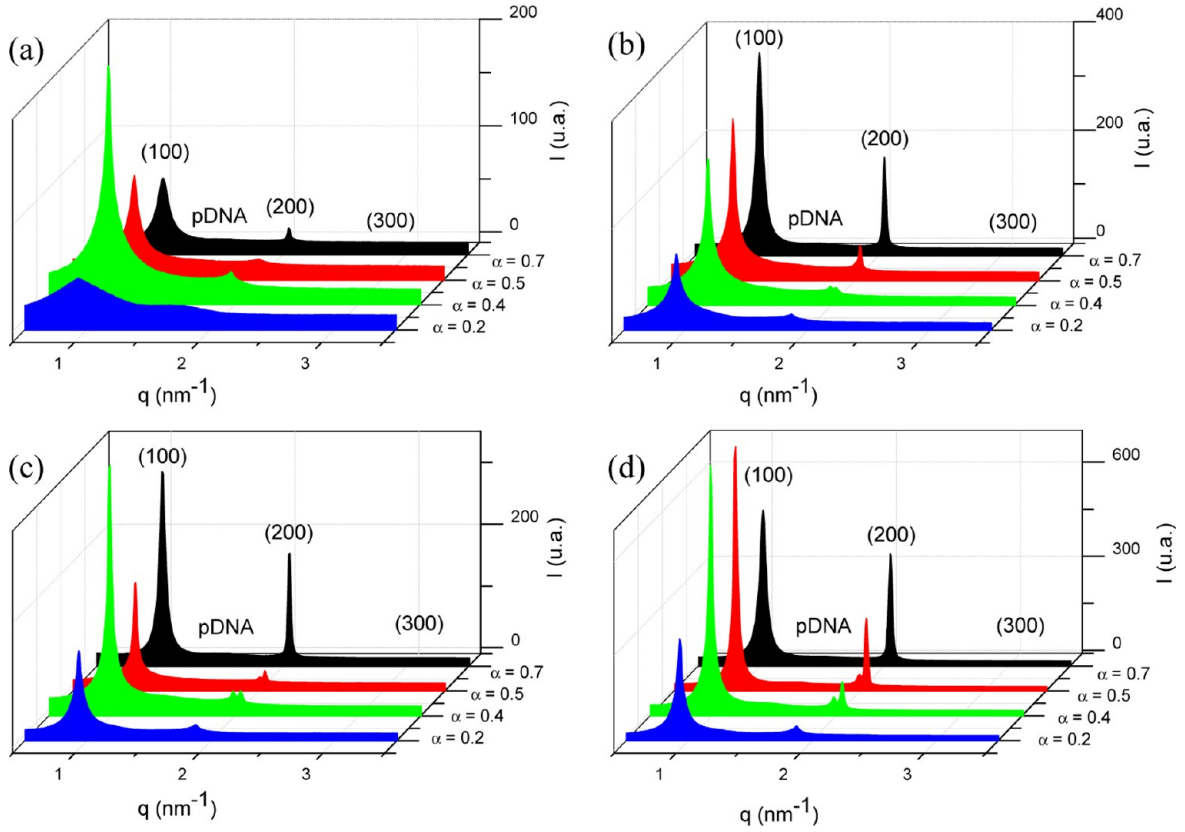

Figure 2. SAXS diffractograms of $(C_{16}Im)_2C_2$/DOPE-pDNA lipoplex nanoaggregates at several CL compositions, α, and effective charge ratios, ρ_{eff}: (a) ρ_{eff} = 1.5, (b) ρ_{eff} = 2.0, (c) ρ_{eff} = 2.5, (d) ρ_{eff} = 3.0.

followed, that is based in a final pass of the mixed liposome solution through a membrane with pores of 100 nm diameter.

SAXS experiments were run for the $(C_{16}Im)_2C_n$/DOPE-pDNA nanoaggregates positively charged ($\rho_{eff} > 1$), covering the whole CL composition, α, and at a wide range of effective charge ratios, ρ_{eff} ($1.5 \leq \rho_{eff} \leq 5.0$). As an example, Figure 2a–d shows the intensity versus q factor of the $(C_{16}Im)_2C_2$/DOPE-pDNA lipoplexes with the Miller indices being included in the plot (additional results for $(C_{16}Im)_2C_n$/DOPE-pDNA lipoplexes, with n = 3, 5, or 12, are given in Figures S-4 to S-6 of the SI). Most of the diffractograms show three peaks that index well to a lamellar structure with the interlayer distance, d, directly related to the q factor ($d = 2\pi/q_{100}$), Based on this, lipoplex nanoaggregates may be represented as alternating bilayers of mixed lipids and an aqueous layer containing pDNA, with thicknesses represented by d_m and d_w, respectively (see Scheme 2, where $d = d_m + d_w$).[20,58−60] The broad and smoothed Bragg peak appearing in the middle of the diffractograms arise from the DNA−DNA correlation, and its q_{pDNA} factor drives to the determination of the separation between pDNA in the layer, d_{pDNA} ($= 2\pi/q_{pDNA}$). q, q_{pDNA}, d, and d_{pDNA} values are reported in Table S-2 (see Tables S-3−S-5 for those obtained for the other CLs series with spacer n = 3, 5, or 12). Results indicate that the lamellar structure at the DOPE rich region (α = 0.2) has higher d values than the lamellar one found in the CL rich region (α = 0.7). In addition, some diffractograms (mostly at intermediate CL compositions, i.e., α = 0.4 and 0.5) show other peaks different than those previously assigned to a lamellar structure, as can be seen in Figure 3b,c, where attention must be focused at a particular effective charge ratio (ρ_{eff} = 2.0). These remaining peaks index well with an additional lamellar structure coexisting with the previous ones. Based on that, we have assigned the peaks to three lamellar structures, one named $L_{\alpha,DOPE\text{-}rich}$ at the DOPE-rich region (red values in Tables S-2−S5 of SI), a second one named $L_{\alpha,main}$ at intermediate CL compositions (black values in Tables S-2−S-5 of SI), and a third one named $L_{\alpha,CL\text{-}rich}$ at the moderate-to-high CL-rich region (blue values in Tables S-2−S-5 of SI). Structural parameters of all the lamellar structures found at any α and ρ_{eff} are given in the SI (Tables S-2−S-5). It may be mentioned that the phenomena of lipid demixing, as shown in this work driving to two sets of coexisting lamellar structures, is not new because such a behavior was already found elsewhere[61] in the DOTAP/DOPC-linear DNA lipoplexes at the helper lipid rich region (α = 0.2), and also found by us more recently in the $(C_{16}Am)_2C_n$/DOPE-pDNA lipoplexes at the whole CL composition, where, in some cases, not only two but even three coexisting lamellar

Scheme 2. Schematic Structure of the $(C_{16}Im)_2C_n$/DOPE-pDNA Lipoplex-Type Nano-Aggregates: (a) Lamellar, L_α, and (b) Inverted Hexagonal, H_{II}^c[a]

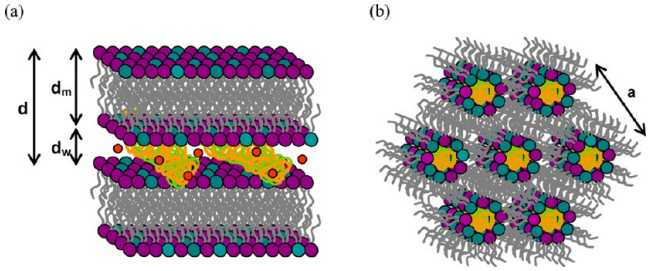

[a]Plasmid DNA (orange-green); Na^+ (red balls).

dx.doi.org/10.1021/bm401079h | Biomacromolecules 2013, 14, 3951−3963

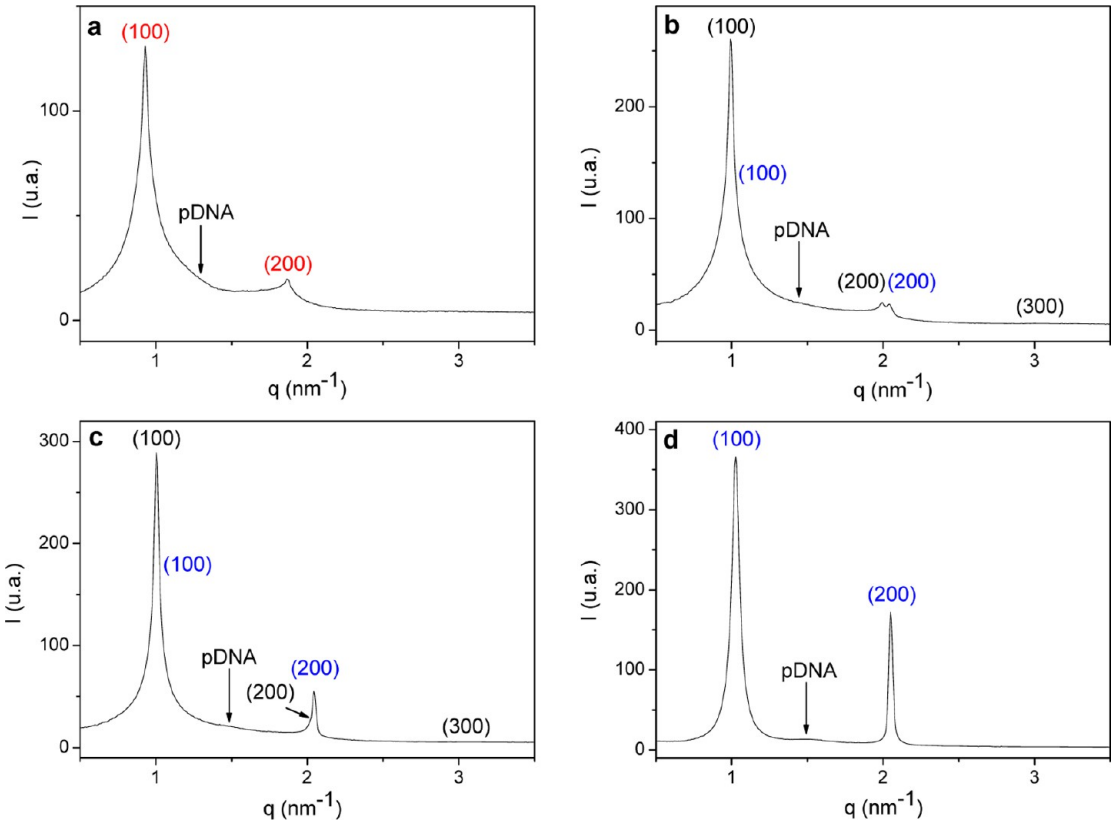

Figure 3. SAXS diffractograms of $(C_{16}Im)_2C_2$/DOPE-pDNA lipoplex nanoaggregates at several CL compositions, α, and at an effective charge ratio ρ_{eff} = 2.0, showing the coexistence of different lamellar L_α structures: $L_{\alpha,main}$ (black), $L_{\alpha,DOPE\text{-}rich}$ (red), and $L_{\alpha,CL\text{-}rich}$ (blue); (a) α = 0.2, (b) α = 0.4, (c) α = 0.5, and (d) α = 0.7.

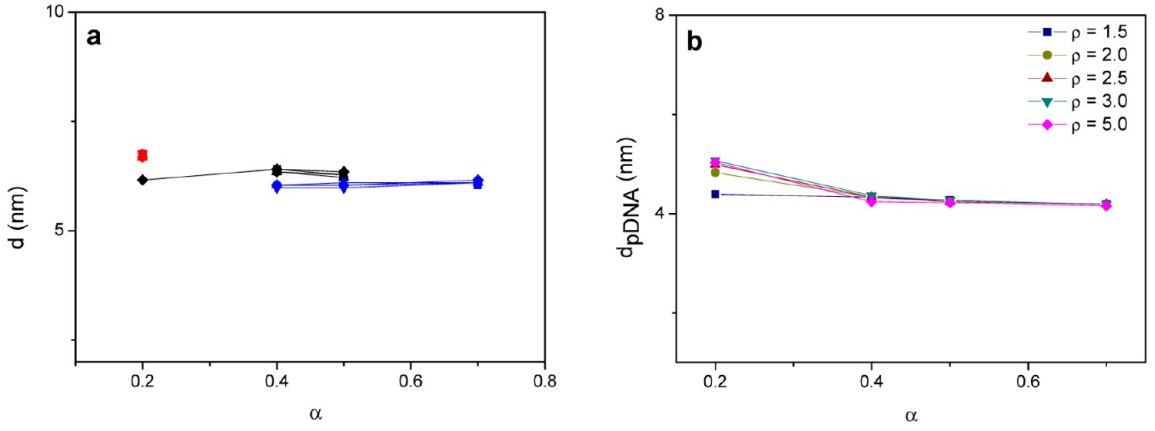

Figure 4. (a) Plots of the periodic distance of the lamellar structure, d, for $(C_{16}Im)_2C_2$/DOPE-pDNA lipoplex nanoaggregates as a function of CL composition, α, at several effective charge ratios, ρ_{eff}: red symbols, $L_{\alpha,DOPE\text{-}rich}$ structure; black symbols, $L_{\alpha,main}$ structure; and blue symbols, $L_{\alpha,CL\text{-}rich}$ structure. In all the structures, ρ_{eff} is squares, 1.5; circles, 2.0; up triangles, 2.5; down triangles, 3.0; and diamonds, 5.0. (b) Plots of the distance d_{pDNA} for $(C_{16}Im)_2C_2$/DOPE-pDNA nanoaggregates as a function of CL composition, α, at several effective charge ratios, ρ_{eff}.

structures were found.[20] Figures 4a and S-8(a1,b1,c1) of SI show plots of the periodic distance of the three lamellar structures, d, versus α, at all ρ_{eff} values for the four $(C_{16}Im)_2C_n$/DOPE-pDNA lipoplexes. As can be seen, the distance, d, of the three lamellar structures remains independent of the CL composition, α, and follow the trend ($d_{L_{\alpha,DOPE\text{-}rich}} \approx 6.5-7.0$ nm) > ($d_{L_{\alpha,main}} \approx 6.0-6.5$ nm) > ($d_{L_{\alpha,CL\text{-}rich}} \approx 5.5-6.0$ nm). Such behavior may be attributed to a combination of several factors: (i) a thinner bilayer, d_m, as α increases, because the length of the $(C_{16}Im)_2C_n$ gemini surfactants is a little shorter than that of DOPE, and (ii) a thicker aqueous layer, d_w, in the DOPE-rich region (low charged bilayers) together with a low presence of negative pDNA, which results in a less degree of compaction. Thus, the compaction of pDNA increases with the positive charge of the bilayer, that is, with α. Considering that $d_m \approx$ 4.0–4.5 nm (determined from cryo-TEM micrographs, as detailed later), the thickness obtained for the pDNA layer ($d_w \approx$ 2.0 nm))[19,20] is consistent with a highly compacted pDNA conformation compared with linear ctDNA ($d_w \approx$ 2.5 nm).[3,7,26] Although it is known[21,26] that the presence of high quantities of DOPE helper lipid in the mixed liposome (i.e., low α values)

dx.doi.org/10.1021/bm401079h | Biomacromolecules 2013, 14, 3951–3963

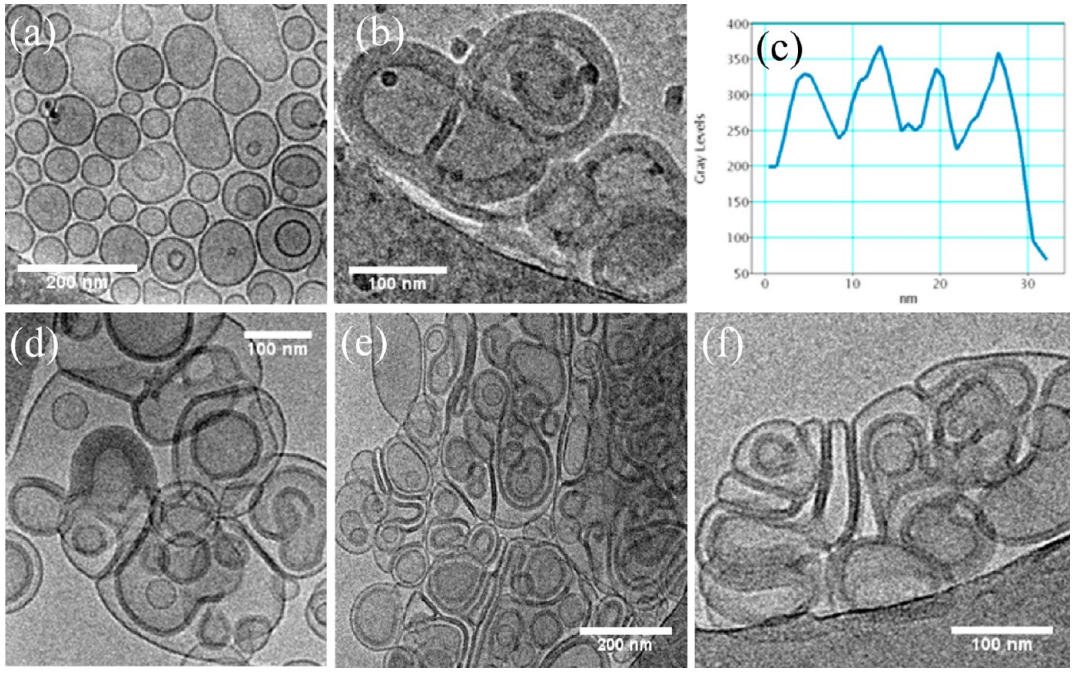

Figure 5. Selection of cryo-TEM micrographs showing a general view of the $(C_{16}Im)_2C_n$/DOPE liposomes (panel a) and $(C_{16}Im)_2C_n$/DOPE-pDNA lipoplex nanoaggregates (panels b–f), all at α = 0.2: (b, c) n = 2, (d) n = 3, (e) n = 5, and (f) n = 12. Plots of the gray level vs distance across the multilamellae of nanoaggregates shown on panel b are shown in panel c. Scale bars are 200 nm in panels a and e, and 100 nm in panels b, c, d, and f.

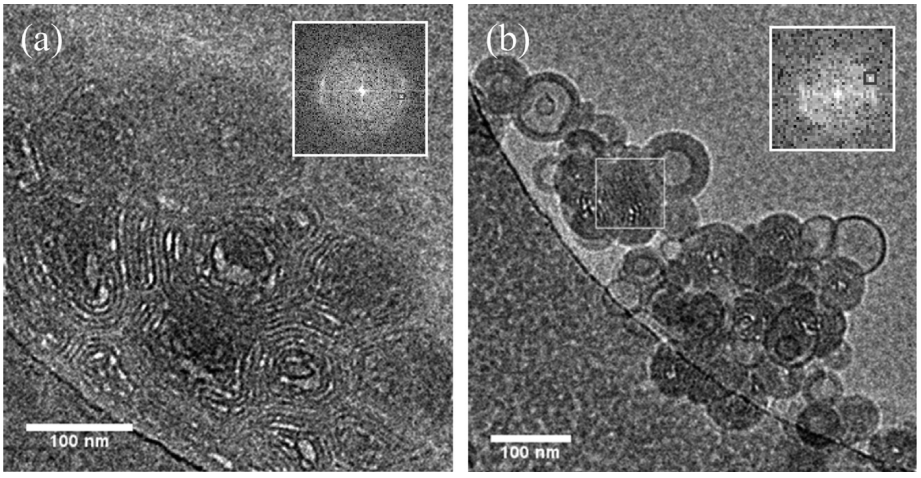

Figure 6. Selection of cryo-TEM micrographs showing a general view of the $(C_{16}Im)_2C_n$/DOPE-pDNA lipoplex nanoaggregates, all at α = 0.5: (a) n = 2 and (b) 5. Insets on panels show the diffraction spots from FFT calculations over a selected area on the original micrograph. FFT pattern reveals a multilamellar structure, with a periodicity of 6.5 ± 0.2 nm on average. Scale bars are 100 nm.

favors the formation of an inverted hexagonal structure, H_{II}^c (see Scheme 2), no inverted hexagonal structure has been found in the diffractograms analyzed for $(C_{16}Im)_2C_n$/DOPE-pDNA lipoplexes with n = 2, 3, or 5. Nevertheless, at $\alpha \leq 0.5$ some diffractograms of the $(C_{16}Im)_2C_{12}$/DOPE-pDNA series index well with a H_{II}^c structure (see Figure S-7 of SI, as two examples), and at α = 0.2 and ρ_{eff} = 2.5 even two coexisting H_{II}^c structures have been found. The values of q and d (= a = d_{pDNA} = $4\pi/(3q_{10})^{1/2}$) for these H_{II}^c structures are reported in Table S-5 of SI. Figure S-8(c1) also reports the periodic distance, d (= a = d_{pDNA}), of the two inverted hexagonal, H_{II}^c, structures found in the DOPE-rich region of the $(C_{16}Im)_2C_{12}$/DOPE-pDNA lipoplexes. The d values for both H_{II}^c structures are higher than those obtained in the lamellar ones in agreement to that was usually reported in literature[22,26,27,62] for other kind of lipoplex nanoaggregates showing a H_{II}^c structure. The values of d_{pDNA} for all the $(C_{16}Im)_2C_n$/DOPE-pDNA lipoplexes with n = 2, 3, 5, or 12 are plotted against the CL composition, α, in Figures 4b and S-8(a2,b2,c2) of SI. These d_{pDNA} values range from 5.0 to 4.0 nm and show a slight decrease with α for all the lipoplexes and at all the effective charge ratios, ρ_{eff}, given that, at constant charge ratio, d_{pDNA} should decrease as the CL composition, α, in the lipoplex nanoaggregate increases. In any case, d_{pDNA} values of the lamellar structures (≈ 4.5 nm) are much lower than those for the H_{II}^c hexagonal structures (≈ 7.5 nm), similar to what has been previously reported for other kind of lipoplexes.[20,27,60,63,64]

Cryo-TEM experiments were run on mixed liposomes (see Figure 5a) and on positively charged $(C_{16}Im)_2C_n$/DOPE-pDNA lipoplexes, n = 2, 3, 5, or 12 (see Figure 5b–f, for α =

0.2 and in Figures 6 and S-9, for α = 0.5). The analysis of the micrographs in Figure 5a and others (not shown) indicates that liposomes studied herein are mostly unilamellar and spherical, with average diameters around 92 ± 10 nm and a lipid bilayer of 4.5 ± 0.3 nm width on average, in very good agreement with the sizes determined by the PALS technique. These liposomes compact pDNA efficiently onto their cationic surfaces and cryo-TEM micrographs reported in Figures 5, 6, and S-9 reveal that the resulting lipoplex-type nanoaggregates are characterized by a multilamellar compaction pattern, consisting of a series of cationic lipidic bilayers with pDNA sandwiched between them, similarly to other lipoplexes previously studied by us.[20,27,56,65] However, two different multilamellar types of complexation may be noticed, shown in Figure 5b−f for lipoplex nanoaggregates with a rich content on DOPE (α = 0.2) and presented by lipoplexes with a higher CL content (α = 0.5), as reported in Figures 6 and S-9. Thus, in the rich-DOPE region, that is, at α = 0.2, the presence of pDNA induces aggregation, leading to the formation of cluster-like nanostructures (CT-type nanoaggregates), where the mixed liposomes are deformed at the surface of the contact with the adjacent liposomes. Notice, however, that when the CL content increases (α = 0.5), in addition to these CT-type nanoaggregates, one can observe the presence of regions with a continuum arrangement of multilamellae with pDNA sandwiched among them, following a typical fingerprint pattern (FP-type nanoaggregates). It seems that when the content on DOPE is high, the liposomes compact superficially the plasmid, essentially keeping their forms; their lipid bilayers thicken and twist or even loop, but the mixed liposome is not disrupted. However, when the content on CL increases, liposome-pDNA interaction is clearly favored and liposomes tend to disrupt in order to form these FP-type nanoaggregates. In conclusion, at α = 0.2, only one type of multilamellar structure, the CT-type, is found, while both CT- and FP- lamellar phases coexist, at α = 0.5, in concordance with what have been also found in SAXS where the $L_{\alpha,\text{DOPE-rich}}$ structure has been assigned at α = 0.2, while $L_{\alpha,\text{main}}$ and $L_{\alpha,\text{CL-rich}}$ phases have been indexed at α = 0.5, particularly for $(C_{16}Im)_2C_n$/DOPE-pDNA lipoplex samples with n = 2, 3, or 5. Some of those CT multilamellar structures were chosen to analyze the periodicity pattern that would confirm the regular arrangement of the multilamellae (see details of the image processing protocol in the SI). Figure 5c shows a plot of gray levels vs distance for the $(C_{16}Im)_2C_2$/DOPE-pDNA lipoplexes at α = 0.2, as an example. Several peaks, related to the level of electronic density can be observed in the plots, reveal the existence of multilayers whose interlamellar distance may be calculated by measuring the distance between the maxima. Accordingly, similar average interlamellar spacings of 6.9 ± 0.2, 6.7 ± 0.2, 6.9 ± 0.2, and 6.7 ± 0.2 nm were obtained for $(C_{16}Im)_2C_n$/DOPE-pDNA with n = 2, 3, 5, or 12, respectively, confirming the compaction of pDNA on a lamellar structure. On the other hand, FP-type nanostructures of Figures 6 and S-9 have been also analyzed with FFT protocols, in order to confirm their multilamellar (L_α phases) character. The insets of Figure 6a,b show a typical FFT profile where the diffraction spots correspond to a lamellar pattern with a periodicity of 6.7 ± 0.2 nm and confirm that the FP-type nanoaggregates are also due to a multilamellar arrangement of CLs and pDNA. This fingerprint pattern, associated with a multilamellar nanoaggregation is also documented in literature for lipoplexes of linear DNA and monomeric CLs.[66−70] The average values obtained for the interlamellar distance of CT and FP-type multilamellar nanoaggregates indicate that there is no appreciable difference on pDNA compaction among both multilamellar patterns, irrespectively of the spacer length of the gemini lipid, and in agreement to those found from SAXS diffractograms for the lamellar structures at α = 0.2 and α = 0.5, specially for those containing CLs with shorter spacers. Nevertheless, one must note that the CT-type structures contain 4−7 lamellae, while the FP-types show a higher number of lamellae.

Not only the structure, morphology, and dimensions of the lipid bilayer, but also its fluidity are factors that affect their potential as DNA carriers and their capability as transfecting agents. In fact, fluidity of the lipid bilayer is a biophysical parameter that is known to have important implications on the transfection efficiency of the gene vector.[4,71,72] Among others, fluorescence anisotropy, r, can be used as a measurement of the fluidity of the bilayer since, as long as bilayer becomes more fluid, the degree of rotation of an excited fluorescent probe placed within must increase and, accordingly, anisotropy of the probe decreases. Figure S-10 of SI shows anisotropy values of the DPH fluorophore located in the bilayer of the $(C_{16}Im)_2C_n$/DOPE liposomes, in the absence ($\rho_{\text{eff}} = \infty$) and in the presence of pDNA, as a function of temperature. It may be noticed that the fluidity of the lipid bilayer increases in all cases, in agreement with what has been previously reported[4,22,26,27,56,62,73] for other lipoplexes, where DOPE is used as a helper lipid. It is also known that DOPE increases liposome fluidity, due in part to its low gel-to-fluid transition temperature, T_m, that reduces T_m of the mixed liposome below room temperature.[4,56] Given that no change on the slope of r versus T profiles has been observed, it may be concluded that T_m of $(C_{16}Im)_2C_n$/DOPE liposomes are below the experimental temperature range studied, which confirms that liposome and lipoplex bilayers are in the fluid state at physiological temperature. All the plots indicate that the presence of pDNA (at different ρ_{eff}) does not modify anisotropy versus T profiles of liposomes ($\rho_{\text{eff}} = \infty$). Similar results have been reported for other lipoplexes.[4,56] Transfection efficiency is known to be influenced by the bilayer fluidity of the lipoplexes since in the gel-like phase the cationic lipid aggregates are not flexible enough to allow for efficient pDNA interaction. At this respect, anisotropy levels lower than 0.2−0.25 are believed to be related with fluid structures capable of allowing a potentially efficient transfection.[74] Based on that, although the presence of pDNA in the lipoplex-type nanoaggregate increases scarcely the anisotropy (see Figures S-10 of SI), in the four systems, at all the CL compositions, α, and effective charge ratios, ρ_{eff}, the anisotropy values are lower than 0.25 in all the cases, indicating that the fluidity of the lipoplexes examined in this study remains high enough to consider these nanoaggregates potentially efficient as transfecting agents of pDNA.

Transfection Efficiency and Cell Viability. Measurement of TE of mixed lipids $(C_{16}Im)_2C_n$/DOPE with n = 2, 3, 5, or 12 across HEK293T cells were performed both in absence (-FBS-FBS) and presence (-FBS+FBS) of serum. This study was carried out using a wide range of CL composition, α, and the effective charge ratio, ρ_{eff}, of the lipoplexes. The results were obtained using a flow assisted cell sorting (FACS) method that permits the determination of the proportion of transfected cells as the percentage of the protein (% GFP) and the mean fluorescence intensity (MFI) into the cells. A high MFI value indicates high level of GFP protein expression per cell which

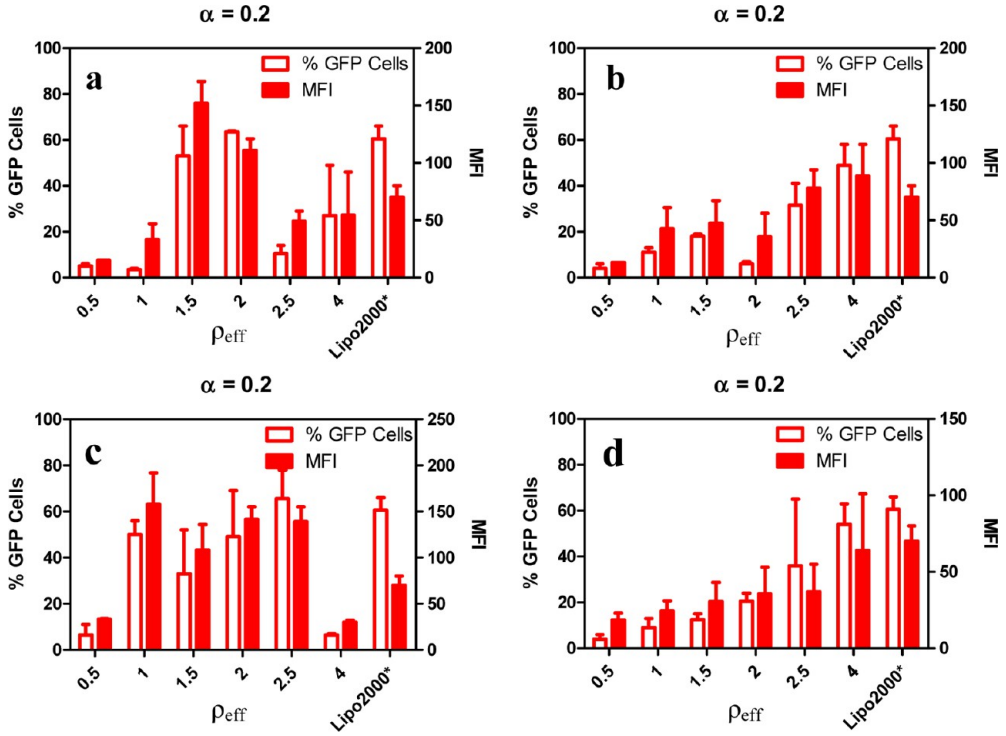

Figure 7. Transfection of pEGFP-C3 in HEK293T cells in presence of serum (-FBS+FBS) using lipoplex nanoaggregates at $\alpha = 0.2$ and $\rho_{eff} = 0.5$, 1, 1.5, 2, 2.5, and 4 of (a) $(C_{16}Im)_2C_2$/DOPE-pDNA; (b) $(C_{16}Im)_2C_3$/DOPE-pDNA; (c) $(C_{16}Im)_2C_5$/DOPE-pDNA, and; (d) $(C_{16}Im)_2C_{12}$/DOPE-pDNA. Experiments were performed using 0.8 μg pDNA per well. Lipoplexes were incubated for 6 h and analyzed after 48 h of incubation at ambient condition. Lipo2000* was used as a positive control.

occurred because of the high copy number of pDNA transfected, transcripted, and translated per cell, while % GFP cells indicates percentage of cell population expressing GFP protein.

Initially, all the lipoplex compositions were optimized for transfection of pDNA in absence of serum condition (-FBS-FBS) in HEK293T cells. It was found that lipoplex $(C_{16}Im)_2C_2$/DOPE-pDNA (Figure S-10) at $\alpha = 0.2$ gave a bell shaped bar diagram with increasing ρ_{eff}, which found maximum for 1.5 with ~65% GFP positive cells having ~190 MFI, whereas at $\alpha = 0.4$ maximum was achieved for $\rho_{eff} = 2.5$ and which again dropped back to $\rho_{eff} = 2$ and 1.5 in case of $\alpha = 0.5$ and 0.7, respectively. Although the % GFP cells and MFI were found to decrease with increasing mole fraction of CL in lipid mixture $(C_{16}Im)_2C_2$/DOPE, that is, increasing α value. Similarly, $(C_{16}Im)_2C_3$/DOPE-pDNA lipoplex showed a decrease in % GFP cells and MFI with increasing α value, while maximum of ~50% GFP positive cells with ~150 MFI was reported at $\rho_{eff} = 2.5$ of $\alpha = 0.2$ (Figure S-11). An unexpectedly high transfection with %GFP cells ~60 and MFI ~300 was reported in case of $(C_{16}Im)_2C_5$/DOPE-pDNA lipoplex at $\rho_{eff} = 1$ of $\alpha = 0.2$, although the pattern of decreasing transfection with increasing α values from 0.2 to 0.7 remained the same, as in the case of previously discussed CLs (Figure S-12). On the other hand, lipoplex $(C_{16}Im)_2C_{12}$/DOPE-pDNA show considerable low TE in the series and did not show any particular pattern in TE variation along with variation in values of ρ_{eff} for various α values (Figure S-13). Overall, TE of CL mixtures was found to decrease from $(C_{16}Im)_2C_2$ to $(C_{16}Im)_2C_3$, which increased a gain in case of $(C_{16}Im)_2C_5$ and further decreased for $(C_{16}Im)_2C_{12}$. It gave a decreasing pattern of optimized TE as $(C_{16}Im)_2C_2$ > $(C_{16}Im)_2C_5$ > $(C_{16}Im)_2C_3$ > $(C_{16}Im)_2C_{12}$. In all the cases, Lipo2000 was used as positive control, transfecting ~60% cells with MFI of ~150, which was considerably lower than the ~65% GFP positive cells having ~190 MFI obtained in case of lipoplex $(C_{16}Im)_2C_2$/DOPE-pDNA at $\rho_{eff} = 1.5$ of $\alpha = 0.2$ and % GFP cells ~60 and MFI ~300 from $(C_{16}Im)_2C_5$/DOPE-pDNA lipoplex at $\rho_{eff} = 1$ of $\alpha = 0.2$.

Further TE was measured in presence of 10% serum (-FBS +FBS) condition. In the case of lipoplex $(C_{16}Im)_2C_2$/DOPE-pDNA, a bell-shaped pattern was seen in TE on increasing ρ_{eff}, while maximum efficiency was attained at $\rho_{eff} = 1.5$ of $\alpha = 0.2$ showing ~70% cells GFP positive with ~175 MFI. At $\alpha = 0.4$ and 0.5, the TE was found to be increasing with increase in ρ_{eff} from 0.5 to 4, but was considerably low compared to the TE at $\rho_{eff} = 1.5$ of $\alpha = 0.2$ (Figure S-14). A pattern of increasing TE with increasing ρ_{eff} was reported across all the α compositions of lipoplex $(C_{16}Im)_2C_3$/DOPE-pDNA, too (Figure S-15), while maximum efficiency was observed at $\rho_{eff} = 4$ of $\alpha = 0.2$ with ~50% GFP positive cells having ~100 MFI. Again an upsurge in TE was seen in case of lipoplex $(C_{16}Im)_2C_5$/DOPE-pDNA at $\rho_{eff} = 2.5$ of $\alpha = 0.2$ exhibiting ~70% GFP positive cells with considerably high MFI of ~150 (Figure S-16). The TE was found to be decreasing with increase in values of α from 0.2 to 0.7, while for a particular α, increase in ρ_{eff} causes increase in TE from 0.5 to 2.5, which further drops down in case of $\rho_{eff} = 4$. Further TE in case of $(C_{16}Im)_2C_{12}$/DOPE-pDNA lipoplex was found to be invariable across the value of α from 0.2 to 0.7, while for a particular α, an increase in ρ_{eff} causes an increase in TE from 0.5 to 4 (Figure S-17). Thus, even in the presence of serum, the pattern of TE for CL mixtures was found to decrease from $(C_{16}Im)_2C_2$ to $(C_{16}Im)_2C_3$, which increased gain in case of $(C_{16}Im)_2C_5$ and further decreased for $(C_{16}Im)_2C_{12}$,

dx.doi.org/10.1021/bm401079h | Biomacromolecules 2013, 14, 3951−3963

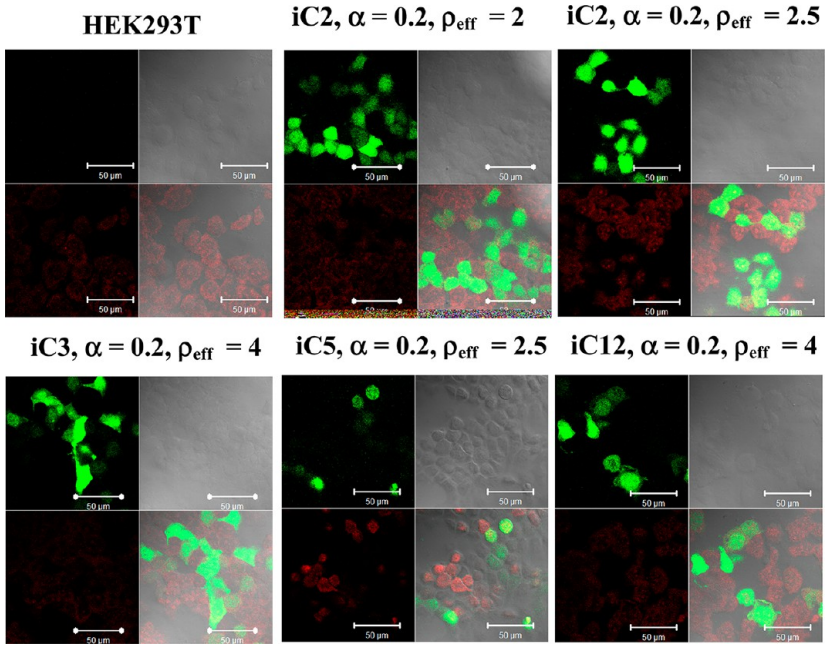

Figure 8. Representative confocal images of HEK293T cells transfected with various lipoplex nanoaggregates [$(C_{16}Im)_2C_n$/DOPE-pDNA] prepared at optimized α and ρ_{eff} values in absence of serum (-FBS-FBS). Here iC2, iC3, iC5, and iC12 represent gemini lipid $(C_{16}Im)_2C_2$, $(C_{16}Im)_2C_3$, $(C_{16}Im)_2C_5$, and $(C_{16}Im)_2C_{12}$, respectively. Experiments were performed using 0.8 μg pDNA per well. (A1-A4) Negative control (cells only); cells incubated with the four lipoplexes: B1−B4 with iC2, C1−C4 with iC2, D1−D4 with iC3, E1−E4 with iC5, and F1−F4 with iC12. Panels A1, B1, C1, D1, E1, and F1 show the GFP in cell, whereas A2, B2, C2, D2, E2, and F2 show the phase contrast of the cells. Panels A3, B3, C3, D3, E3, and F3 show propidium iodide stain, whereas A4, B4, C4, D4, E4, and F4 are overlaps of panels 1 and 3 in each case. Scale bars are 50 nm.

creating a decreasing pattern of optimized TE as $(C_{16}Im)_2C_2$ > $(C_{16}Im)_2C_5$ > $(C_{16}Im)_2C_3$ > $(C_{16}Im)_2C_{12}$ (Figure 7). In all the cases, Lipo2000* (Lipo2000 in presence of 10% serum) was used as a positive control which gave ∼55% GFP positive cells with MFI of ∼70, which was considerably lower than the ∼70% GFP positive cells having ∼175 MFI obtained in case of lipoplex $(C_{16}Im)_2C_2$/DOPE-pDNA at ρ_{eff} = 1.5 of α = 0.2, and %GFP cells ∼65 and MFI ∼150 from $(C_{16}Im)_2C_5$/DOPE-pDNA lipoplex at ρ_{eff} = 1 of α = 0.2. Thus, we could generate lipoplexes of various CLs [$(C_{16}Im)_2C_n$ (where n = 2, 3, 5, or 12)] mixed with DOPE at α = 0.2 and various ρ_{eff} to get high TE in presence of 10% serum in HEK293T cells (Figure 7).

The analysis arising from the biophysical and biochemical approaches presented and discussed in the previous sections may be used to establish a structure-biological activity relationship of the formulations studied herein. The best formulations to transfect pDNA are reported with gemini CLs with shorter spacers at low α composition of the mixed liposome and at moderate effective charge ratios, ρ_{eff}, of the lipoplexes. It was already found in lipoplexes formed with other gemini CLs with similar spacer lengths[20] that short spacers give the appropriate distance between the two cationic headgroups to interact better with the pDNA negative charges while moderate effective charge ratios (in the range 1.5−5) imply the minimum positive charge lipoplex able to transfect pDNA at the lowest cytotoxicity. On the other hand, optimum TE at low CL composition (α = 0.2), that is, at the DOPE-rich region, is in agreement with several positive factors: (a) the fusogenic character of DOPE with cells membrane and (b) the presence, in most cases, of two coexisting lamellar structures found with SAXS and confirmed with cryo-TEM, that could synergize the transfection. Furthermore, the CT-type lamellar structure found by cryo-TEM at α = 0.2, with 4−7 lamellae, is expected to release pDNA easier from the lipoplex (thus enhancing transfection) compared with the FP-type lamellar structure found at α = 0.5, that is formed by many more lamellae. Finally, hexagonal structures found in the CL-DOPE systems at low α values are usually related to a high transfection efficiency,[59,75] but in the series reported in this work, the H_{II}^c hexagonal structures have been found only for the $(C_{16}Im)_2C_{12}$/DOPE-pDNA lipoplex, where the CL has the longest spacer studied here, which, in turn, is just the one that shows the lowest transfection of the series. For that reason, the hexagonal structures found herein, although could favor the TE, are not able to counterbalance the low TE due to the CL with the longest spacer.

To generalize these TE results, those lipoplexes that showed optimum TE values in HEK293T cells were used to perform transfection experiments in a few other cell lines, namely, HeLa, H1299, H460, A549, and NIH3T3 (Figure S-18) in the presence of serum (-FBS+FBS). Experiments were performed using ρ_{eff} = 0.5, 1, 1.5, 2, 2.5, and 4 of $(C_{16}Im)_2C_2$/DOPE-pDNA lipoplex; 4 of $(C_{16}Im)_2C_3$/DOPE-pDNA; 2.5 of $(C_{16}Im)_2C_5$/DOPE-pDNA; and 4 of $(C_{16}Im)_2C_{12}$/DOPE-pDNA, at α = 0.2 for all. It was found that lipoplex $(C_{16}Im)_2C_2$/DOPE-pDNA at ρ_{eff} = 1.5 was a better transfecting agent than the Lipo2000* in HeLa and HEK293T cells, while ρ_{eff} = 2.5 was better than Lipo2000* in H1299 cells. On the other side, in H460, A549, and NIH3T3 cells, TE was achieved only comparable to Lipo2000* at best optimized α and ρ_{eff} for different lipoplexes.

The structure and TE of these lipoplexes would have been significantly influenced by the presence of serum proteins while performing the transfection experiments in serum. It has been well studied that variation in TE of lipids in serum influenced by the serum−lipoplex interaction. Toward this, it has been reported that serum proteins compete for the cationic surface of lipid membranes leading to the formation of a "protein

dx.doi.org/10.1021/bm401079h | Biomacromolecules 2013, 14, 3951−3963

corona",[76] which may help them to easily release their DNA payload at the desired location.[77] This protein corona significantly changes the surface chemistry of nanoparticles based on the presence of neutral lipids, viz. DOPE and cholesterol and decide their bioidentity via molecular characteristics, arrangement, and residence time of the proteins in the dynamic ensemble.[78−81] Thus, the structural features of the lipoplexes in presence of serum and individual serum proteins could be manifested.

These $(C_{16}Im)_2C_n$/DOPE-pDNA lipoplex-type nanoaggregates have been found to be overall better agents for the gene transfection compared to the corresponding ammonium ion based $(C_{16}Am)_2C_n$/DOPE-pDNA lipoplexes, recently studied by our group.[20] As in case of $(C_{16}Am)_2C_n$/DOPE-pDNA, the TE for a particular CL across the various α and ρ_{eff} values was varied to a very high or low extent with no fixed pattern whereas $(C_{16}Im)_2C_n$/DOPE-pDNA gave a lot better pattern of increase and decrease in TE. Probably, the presence of delocalized positive charge on the imidazolium headgroup plays an important role in DNA binding and release efficiency of this imidazolium headgroup of $(C_{16}Im)_2C_n$ lipids. The presence of aromatic π-electrons in the headgroup region probably allows the additional $\pi-\pi$ interactions with the DNA bases and the imidazolium headgroups during the lipoplex formation. This additional stabilizing interaction might be helpful in controlling both the DNA binding and release efficiency of these $(C_{16}Im)_2C_n$ lipids in different way, which in turn probably helps in the manifestation of higher TE. On the other hand, in $(C_{16}Im)_2C_n$ lipoplexes, pDNA exposes less effective negative charge, and requires less quantity of $(C_{16}Im)_2C_n$ compared to $(C_{16}Am)_2C_n$ to generate a stable lipoplex. This is particularly true especially for the gemini CLs with shorter spacer with higher % of DOPE, that is, $n = 2$ at $\alpha = 0.2$[20] Probably, a lower amount of CL in the lipoplex composition reduces the interactions between the anionic serum proteins and CL and results in an improvement in the overall TE.

The transfection efficiency of each prepared lipoplex has been also measured using a confocal fluorescence microscopy study. This method was used to visualize the level of GFP expression inside the cells 48 h post-transfection. In this technique, the nucleus of the cells has been stained (red color) with propidium iodide (PI) due to the presence of endogenous DNA present in cells to begin with while green fluorescence appeared because of the expressed GFP. We could see highly fluorescent GFP positive HEK293T cells after transfection with pDNA in absence (-FBS-FBS; Figure 8) and presence (-FBS +FBS) of serum (Figure S-19) using lipoplex $(C_{16}Im)_2C_2$/DOPE-pDNA at $\rho_{eff} = 1.5$ and 2; $(C_{16}Im)_2C_3$/DOPE-pDNA at $\rho_{eff} = 4$; $(C_{16}Im)_2C_5$/DOPE-pDNA at $\rho_{eff} = 2.5$; and $(C_{16}Im)_2C_{12}$/DOPE-pDNA at $\rho_{eff} = 4$, of $\alpha = 0.2$ in all the cases. These representative images also include GFP expression because of pDNA transfection using Lipo2000* in presence of 10% serum (Figure S-17). In all the cases, cells expressed GFP indicates that %GFP positive cell data obtained from FACS analysis were not a false positive. The images obtained for the optimum $(C_{16}Im)_2C_n$/DOPE-pDNA formulations indicate that the fluorescence intensity due to the expressed GFP follows the trend $(C_{16}Im)_2C_2$/DOPE > $(C_{16}Im)_2C_5$/DOPE > $(C_{16}Im)_2C_3$/DOPE > $(C_{16}Im)_2C_{12}$/DOPE. These observations are in agreement with the data of flow cytometry (FACS) and show that the spacer length, n, of the CL has a moderate effect. In any case, these formulations are similar or, in the case of short-to-medium length spacers, even better than the Lipofectamine2000.

MTT assay experiments were performed on HEK293T cells to find the cell viability (cytotoxicity) of all the lipoplexes at the different CL composition, α, and all the used effective charge ratios, ρ_{eff}. Here results are presented for only two optimum effective charge ratios, ρ_{eff}, where the best TE was found for each CL composition, α. In this assay, the percentage of cells that remained viable to grow and divide after the lipoplex incubation with cells for 6, 24, and 48 h was measurement. It was found that irrespective of the CL composition, α, lipoplex $(C_{16}Im)_2C_2$/DOPE-pDNA showed ∼100% cell viability when incubated for only 6 and 24 h, but a slight decrease in cell viability was reported for 48 h incubation. However, in each and every case, the cell viability was found to be better compared to the condition when cells were incubated with pDNA complexed with Lipo2000 for all three time points (Figure 9). Similarly, for the lipoplexes $(C_{16}Im)_2C_3$/DOPE-pDNA, $(C_{16}Im)_2C_5$/DOPE-pDNA, and $(C_{16}Im)_2C_{12}$/DOPE-pDNA, 6 h incubation did not give any significant toxicity, but 24 and 48 h incubations gave considerable loss in cell viability (Figure S-20). A gradual decrease in cell viability was found with increasing spacer length from 3 to 12 between imidazolium head groups. This observation further shows high feasibility of shorter spacer between imidazolium headgroups for better transfecting agent. Lipo2000 was always more toxic compared to each and every lipoplex formulation used here.

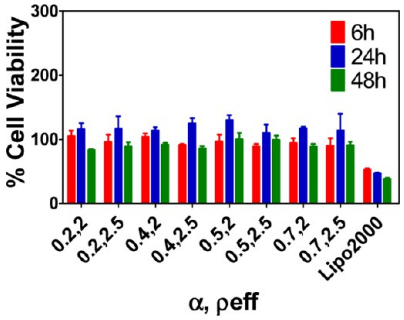

Figure 9. Cell viability assay of $(C_{16}Im)_2C_2$/DOPE-pDNA lipoplex nanoaggregates prepared at various α and ρ_{eff} values in HEK293T cells. Experiments were performed by incubating lipoplexes at different time points of 6, 24, and 48 h. Experiment was performed in the presence of 10% serum (-FBS+FBS). Transfected cells were analyzed after a 48 h incubation.

The cell viability obtained using $(C_{16}Im)_2C_n$/DOPE-pDNA lipoplexes of this work is higher than that was found with $(C_{16}Am)_2C_n$/DOPE-pDNA lipoplexes reported recently.[20] We believe that this high cell viability (lower cytotoxicity) is a result of two factors: (a) a lower toxicity of the imidazolium cationic heads of the CL compared to CL with ammonium cationic heads, and (b) the lowest effective charge of the pDNA, q^-_{pDNA}, and thus, a less quantity of CL used in the appropriate preparation of the lipoplexes at the required effective charges ratios, ρ_{eff}, in the presence of the $(C_{16}Im)_2C_n$/DOPE mixed lipids of this work compared to the $(C_{16}Am)_2C_n$/DOPE ones recently studied.[20]

CONCLUSIONS

We present here the first report that attempts to correlate the morphological variations in lipoplexes of gemini cationic lipids

possessing imidazolium headgroups and how their transfection efficiency is influenced by the variation of spacer length between the two imidazolium headgroups. The biophysical and biological experiments reported here have evidenced that nanoaggregates of DOPE and gemini CLs with two imidazolium headgroups separated by an alkanediyl spacer ($(C_{16}Im)_2C_n$/DOPE) condense, compact, and transfect pEGFP-C3 plasmid DNA (pDNA) efficiently and the spacer length between the two headgroups, the mixed lipid compositions and the lipoplex effective charge ratio hold the key that determine the properties, structure and transfection efficiency of the resulting nanoaggregates. The four gemini lipids ($(C_{16}Im)_2C_n$ with n = 2, 3, 5, or 12), with a nominal charge of +2, have a lower effective charge $q^+_{L^+} = 1.7 \pm 0.1$, while pDNA is compacted, yielding only a 10−25% effective negative charge, q^-_{pDNA}, than that of the linear DNA ($q^-_{DNA} = -2$ per bp). These features demonstrate that compaction and transfection of DNA using mixed CLs requires initially the determination of the effective charges of both the CL and plasmid DNA. SAXS diffractograms of the $(C_{16}Im)_2C_n$/DOPE-pDNA lipoplexes reveal the presence of three types of multilamellar structures, two of them coexist in some CL compositions. Additionally, in the $(C_{16}Im)_2C_{12}$/DOPE-pDNA lipoplex, where the spacer is the longest, two inverted H^c_{II} hexagonal structures were also found in the moderate-to-lower CL composition and at low effective charge ratios. Cryo-TEM micrographs reveal two types (cluster-type and fingerprint-type) of lamellar packing. The cluster-type is observed alone at low α values, while both coexist at moderate α compositions. On transfecting HEK293T cells a decrease in the optimized transfection efficiency was found as $(C_{16}Im)_2C_2$ > $(C_{16}Im)_2C_5$ > $(C_{16}Im)_2C_3$ > $(C_{16}Im)_2C_{12}$. Lipoplex $(C_{16}Im)_2C_2$/DOPE-pDNA at ρ_{eff} = 1.5 of α = 0.2 gave considerably higher transfection than Lipo2000*, not only in HEK293T but also in HeLa and H1299 cells lines. Additionally, the cationic gemini-DOPE mixed formulations reported in this work are highly biocompatible (much better than Lipo2000*) and appear to be safe for use in vitro transformed cell culture and may be extended for the gene therapy studies in vivo, too. It may therefore be concluded that $(C_{16}Im)_2C_n$/DOPE mixed liposomes are adequate and considerably better than Lipo2000* and the CLs of the 1,2-bis(hexadecyl ammonium) alkane series recently reported, as DNA vectors on gene therapy mostly when they consist of a low content of cationic lipid, where the lipoplex forms cluster-type lamellar structures, and when the spacer between the two imidazolium cationic heads of the $(C_{16}Im)_2C_n$ has a short-to-medium length (n = 2 or 5).

■ ASSOCIATED CONTENT

Ⓢ Supporting Information

The procedure related to the synthesis of the divalent cationic gemini surfactants 1,2-bis(hexadecyl imidazolium) alkanes, a full description of all the experimental methods used in the MS, and additional results (figures and tables) needed to analyze the study reported in the MS. This material is available free of charge via the Internet at http://pubs.acs.org.

■ AUTHOR INFORMATION

Corresponding Authors

*Fax: +918023600529. E-mail: sb@orgchem.iisc.ernet.in.
*Fax: +34913944135. E-mail: aicart@quim.ucm.es.

Author Contributions

†These authors contributed equally (S.K.M. and M.M.-Ú.).

Notes

The authors declare no competing financial interest.

■ ACKNOWLEDGMENTS

Authors thank MICINN of Spain (Project Nos. CTQ2009-10002BQU and ACI2009-0867), DST of India (Project No. DST/INT/SPAIN/P-8/2009), and DST for J. C. Bose fellowship to S.B., and Univ. Complutense of Madrid (Spain; Project Nos. UCMA05-33-010 and GR35/10-A). Authors also thank BM26 at ESRF, Grenoble (France), for SAXS experiments, and Servei de Microscopia of Univ. Autónoma of Barcelona (Spain) for cryo-TEM experiments.

■ REFERENCES

(1) Anderson, W. F. *Nature* **1998**, *392*, 25−30.
(2) Yang, Y.; Nunes, F. A.; Berencsi, K.; Goenczoel, E.; Engelhardt, J. F.; Wilson, J. M. *Nat. Genet.* **1994**, *7*, 362−369.
(3) Rädler, J. O.; Koltover, I.; Salditt, T.; Safinya, C. R. *Science* **1997**, *275*, 810−814.
(4) Bhattacharya, S.; Mandal, S. S. *Biochemistry* **1998**, *37*, 7764−7777.
(5) Kirby, A. J.; Camilleri, P.; Engberts, J.; Feiters, M. C.; Nolte, R. J. M.; Soderman, O.; Bergsma, M.; Bell, P. C.; Fielden, M. L.; Rodriguez, C. L. G.; Guedat, P.; Kremer, A.; McGregor, C.; Perrin, C.; Ronsin, G.; van Eijk, M. C. P. *Angew. Chem., Int. Ed.* **2003**, *42*, 1448−1457.
(6) Koynova, R.; MacDonald, R. C. *Biochim. Biophys. Acta* **2007**, *1768*, 2373−2382.
(7) Caracciolo, G.; Marchini, C.; Pozzi, D.; Caminiti, R.; Amenitsch, H.; Montani, M.; Amici, A. *Langmuir* **2007**, *23*, 4498−4508.
(8) Dias, R. S.; Lindman, B. *DNA Interaction with Polymers and Surfactants*; Wiley & Sons: Hoboken, NJ, 2008.
(9) Dileep, P. V.; Antony, A.; Bhattacharya, S. *FEBS Lett.* **2001**, *509*, 327−331.
(10) Ghosh, Y. K.; Visweswariah, S. S.; Bhattacharya, S. *Bioconjugate Chem.* **2002**, *13*, 378−384.
(11) Bajaj, A.; Kondaiah, P.; Bhattacharya, S. *Bioconjugate Chem.* **2007**, *18*, 1537−1546.
(12) Bajaj, A.; Mishra, S. K.; Kondaiah, P.; Bhattacharya, S. *Biochim. Biophys. Acta* **2008**, *1778*, 1222−1236.
(13) Bhattacharya, S.; Dileep, P. V. *Bioconjugate Chem.* **2004**, *15*, 508−519.
(14) Bajaj, A.; Kondaiah, P.; Bhattacharya, S. *Biomacromolecules* **2008**, *9*, 991−999.
(15) Bhattacharya, S.; Bajaj, A. *Chem. Commun.* **2009**, 4632−4656.
(16) Donkuru, M.; Badea, I.; Wettig, S.; Verrall, R.; Elsabahy, M.; Foldvari, M. *Nanomedicine* **2010**, *5*, 1103−1127.
(17) Yang, P.; Singh, J.; Wettig, S.; Foldvari, M.; Verrall, R. E.; Badea, I. *Eur. J. Pharm. Biopharm.* **2010**, *75*, 311−320.
(18) Shirazi, R. S.; Ewert, K. K.; Leal, C.; Majzoub, R. N.; Bouxsein, N. F.; Safinya, C. R. *Biochim. Biophys. Acta* **2011**, *1808*, 2156−2166.
(19) Muñoz-Ubeda, M.; Misra, S. K.; Barran-Berdon, A. L.; Aicart-Ramos, C.; Sierra, M. B.; Biswas, J.; Kondaiah, P.; Junquera, E.; Bhattacharya, S.; Aicart, E. *J. Am. Chem. Soc.* **2011**, *133*, 18014−18017.
(20) Muñoz-Ubeda, M.; Misra, S. K.; Barran-Berdon, A. L.; Data, S.; Aicart-Ramos, C.; Castro-Hartmann, P.; Kondaiah, P.; Junquera, E.; Bhattacharya, S.; Aicart, E. *Biomacromolecules* **2012**, *13*, 3926−3937.
(21) Ewert, K.; Slack, N. L.; Ahmad, A.; Evans, H. M.; Lin, A. J.; Samuel, C. E.; Safinya, C. R. *Curr. Med. Chem.* **2004**, *11*, 133−149.
(22) Lin, A. J.; Slack, N. L.; Ahmad, A.; George, C. X.; Samuel, C. E.; Safinya, C. R. *Biophys. J.* **2003**, *84*, 3307−3316.
(23) Caracciolo, G.; Caminiti, R. *Chem. Phys. Lett.* **2005**, *411*, 327−332.
(24) Caracciolo, G.; Pozzi, D.; Amenitsch, H.; Caminiti, R. *Langmuir* **2005**, *21*, 11582−11587.

(25) Ciani, L.; Casini, A.; Gabbiani, C.; Ristori, S.; Messori, L.; Martini, G. *Biophys. Chem.* **2007**, *127*, 213−220.
(26) Muñoz-Ubeda, M.; Rodriguez-Pulido, A.; Nogales, A.; Martin-Molina, A.; Aicart, E.; Junquera, E. *Biomacromolecules* **2010**, *11*, 3332−3340.
(27) Muñoz-Ubeda, M.; Rodriguez-Pulido, A.; Nogales, A.; Llorca, O.; Quesada-Perez, M.; Martin-Molina, A.; Aicart, E.; Junquera, E. *Soft Matter* **2011**, *7*, 5991−6004.
(28) Barran-Berdon, A. L.; Muñoz-Ubeda, M.; Aicart-Ramos, C.; Perez, L.; Infante, M. R.; Castro-Hartmann, P.; Martin-Molina, A.; Aicart, E.; Junquera, E. *Soft Matter* **2012**, *8*, 7368−7380.
(29) Dobbs, W.; Heinrich, B.; Bourgogne, C.; Donnio, B.; Terazzi, E.; Bonnet, M. E.; Stock, F.; Erbacher, P.; Bolcato-Bellemin, A. L.; Douce, L. *J. Am. Chem. Soc.* **2009**, *131*, 13338−13346.
(30) Kamboj, R.; Singh, S.; Bhadani, A.; Kataria, H.; Kaur, G. *Langmuir* **2012**, *28*, 11969−11978.
(31) Pietralik, Z.; Krzyszton, R.; Kida, W.; Andrzejewska, W.; Kozak, M. *Int. J. Mol. Sci.* **2013**, *14*, 7642−7659.
(32) Huang, Q. D.; Ou, W. J.; Chen, H.; Feng, Z. H.; Wang, J. Y.; Zhu, J. Z. W.; Yu, X. Q. *Eur. J. Pharm. Biopharm.* **2011**, *78*, 326−335.
(33) Mevel, M.; Breuzard, G.; Yaouanc, J. J.; Clement, J. C.; Lehn, P.; Pichon, C.; Jaffres, P. A.; Midoux, P. *ChemBioChem* **2008**, *9*, 1462−1471.
(34) Lv, H. T.; Zhang, S. B.; Wang, B.; Cui, S. H.; Yan, J. *J. Controlled Release* **2006**, *114*, 100−109.
(35) Solodin, I.; Brown, C. S.; Bruno, M. S.; Chow, C. Y.; Jang, E. H.; Debs, R. J.; Heath, T. D. *Biochemistry* **1995**, *34*, 13537−13544.
(36) Gustafsson, J.; Arvidson, G.; Karlsson, G.; Almgren, M. *Biochim. Biophys. Acta* **1995**, *1235*, 305−312.
(37) Lasic, D. D. *Liposomes in Gene Delivery*; CRC Press: Boca Raton, FL, 1997.
(38) Lasic, D. D.; H., S.; Stuart, M. A. C.; R., P.; Frederik, P. *J. Am. Chem. Soc.* **1997**, *119*, 832−833.
(39) Zuidam, N. J.; Barenholz, Y. *Biochim. Biophys. Acta* **1998**, *1368*, 115−128.
(40) Xu, Y. H.; Hui, S. W.; Frederik, P.; Szoka, F. C. *Biophys. J.* **1999**, *77*, 341−353.
(41) Barreleiro, P. C. A.; Olofsson, G.; Brown, W.; Edwards, K.; Bonassi, N. M.; Feitosa, E. *Langmuir* **2002**, *18*, 1024−1029.
(42) Holmberg, K.; Jönsson, B.; Kronberg, B.; Lindman, B. *Surfactants and Polymers in Aqueous Solution*; J. Wiley & Sons: Chichester, England, 2003.
(43) Hirsch-Lerner, D.; Zhang, M.; Eliyahu, H.; Ferrari, M. E.; Wheeler, C. J.; Barenholz, Y. *Biochim. Biophys. Acta* **2005**, *1714*, 71−84.
(44) Feitosa, E.; Alves, F. R.; Niemiec, A.; Oliveira, M.; Castanheira, E. M. S.; Baptista, A. L. F. *Langmuir* **2006**, *22*, 3579−3585.
(45) Salvati, A.; Ciani, L.; Ristori, S.; Martini, G.; Masi, A.; Arcangeli, A. *Biophys. Chem.* **2006**, *121*, 21−29.
(46) Pal, A.; Datta, S.; Aswal, V. K.; Bhattacharya, S. *J. Phys. Chem. B* **2012**, *116*, 13239−13247.
(47) Rodriguez-Pulido, A.; Aicart, E.; Llorca, O.; Junquera, E. *J. Phys. Chem. B* **2008**, *112*, 2187−2197.
(48) Mel'nikov, S. M.; Lindman, B. *Langmuir* **1999**, *15*, 1923−1928.
(49) Barreleiro, P. C. A.; Lindman, B. *J. Phys. Chem. B* **2003**, *107*, 6208−6213.
(50) Dubochet, J.; Adrian, M.; Chang, J. J.; Homo, J. C.; Lepault, J.; McDowall, A. W.; Schultz, P. *Q. Rev. Biophys.* **1988**, *21*, 129−228.
(51) Bednar, J.; Woodcock, C. L. *Chromatin*; Academic Press, Inc.: San Diego, CA, 1999; Vol. *304*, pp 191−213.
(52) Dubochet, J.; Zuber, B.; Eltsov, M.; Bouchet-Marquis, C.; Al-Amoudi, A.; Livolant, F. How to "read" a vitreous section. *Cellular Electron Microscopy*; Elsevier: New York, 2007; Vol. *79*, pp 385−406.
(53) Rodriguez-Pulido, A.; Aicart, E.; Junquera, E. *Langmuir* **2009**, *25*, 4402−4411.
(54) Hansen, M. B.; Nielsen, S. E.; Berg, K. *J. Immunol. Methods* **1989**, *119*, 203−210.
(55) Bajaj, A.; Kondiah, P.; Bhattacharya, S. *J. Med. Chem.* **2007**, *50*, 2432−2442.
(56) Rodriguez-Pulido, A.; Martin-Molina, A.; Rodriguez-Beas, C.; Llorca, O.; Aicart, E.; Junquera, E. *J. Phys. Chem. B* **2009**, *113*, 15648−15661.
(57) Lyubchenko, Y. L.; Shlyakhtenko, L. S. *Proc. Natl. Acad. Sci. U.S.A.* **1997**, *94*, 496−501.
(58) Foldvari, M.; Badea, I.; Wettig, S.; Verrall, R.; Bagonluri, M. *J. Exp. Nanosci.* **2006**, *1*, 165−176.
(59) Pozzi, D.; Caracciolo, G.; Caminiti, R.; De Sanctis, S. C.; Amenitsch, H.; Marchini, C.; Montani, M.; Amici, A. *Appl. Mater. Interfaces* **2009**, *1*, 2237−2249.
(60) Zidovska, A.; Evans, H. M.; Ewert, K. K.; Quispe, J.; Carragher, B.; Potter, C. S.; Safinya, C. R. *J. Phys. Chem. B* **2009**, *113*, 3694−3703.
(61) Koltover, I.; Salditt, T.; Safinya, C. R. *Biophys. J.* **1999**, *77*, 915−924.
(62) Ewert, K. K.; Evans, H. M.; Bouxsein, N. F.; Safinya, C. R. *Bioconjugate Chem.* **2006**, *17*, 877−888.
(63) Farago, O.; Ewert, K.; Ahmad, A.; Evans, H. M.; Gronbech-Jensen, N.; Safinya, C. R. *Biophys. J.* **2008**, *95*, 836−846.
(64) Caracciolo, G.; Pozzi, D.; Amici, A.; Amenitsch, H. *J. Phys. Chem. B* **2010**, *114*, 2028−2032.
(65) Rodriguez-Pulido, A.; Ortega, F.; Llorca, O.; Aicart, E.; Junquera, E. *J. Phys. Chem. B* **2008**, *112*, 12555−12565.
(66) Battersby, B. J.; Grimm, R.; Huebner, S.; Cevc, G. *Biochim. Biophys. Acta* **1998**, *1372*, 379−383.
(67) Huebner, S.; Battersby, B. J.; Grimm, R.; Cevc, G. *Biophys. J.* **1999**, *76*, 3158−3166.
(68) Tarahovsky, Y. S.; Rakhmanova, V. A.; Epand, R. M.; MacDonald, R. C. *Biophys. J.* **2002**, *82*, 264−273.
(69) Rosa, M.; Moran, M. D.; Miguel, M. D.; Lindman, B. *Colloids Surf., A* **2007**, *301*, 361−375.
(70) Rosa, M.; Miguel, M. D.; Lindman, B. *J. Colloid Interface Sci.* **2007**, *312*, 87−97.
(71) Zantl, R.; Baicu, L.; Artzner, F.; Sprenger, I.; Rapp, G.; Rädler, J. O. *J. Phys. Chem. B* **1999**, *103*, 10300−10310.
(72) Aljaberi, A.; Spelios, M.; Kearns, M.; Selvi, B.; Savva, M. *Colloids Surf., B* **2007**, *57*, 108−117.
(73) Safinya, C. R. *Curr. Opin. Struct. Biol.* **2001**, *11*, 440−448.
(74) Regelin, A. E.; Fankhaenel, S.; Gurtesch, L.; Prinz, C.; von Kiedrowski, G.; Massing, U. *Biochim. Biophys. Acta* **2000**, *1464*, 151−164.
(75) Bouxsein, N. F.; McAllister, C. S.; Ewert, K. K.; Samuel, C. E.; Safinya, C. R. *Biochemistry* **2007**, *46*, 4785−4792.
(76) Caracciolo, G.; Callipo, L.; De Sanctis, S. C.; Cavaliere, C.; Pozzi, D.; Lagana, A. *Biochim. Biophys. Acta* **2010**, *1798*, 536−543.
(77) Caracciolo, G.; Pozzi, D.; Capriotti, A. L.; Marianecci, C.; Carafa, M.; Marchini, C.; Montani, M.; Amici, A.; Amenitsch, H.; Digman, M. A.; Gratton, E.; Sanchez, S. S.; Lagana, A. *J. Med. Chem.* **2011**, *54*, 4160−4171.
(78) Barran-Berdon, A. L.; Pozzi, D.; Caracciolo, G.; Capriotti, A. L.; Caruso, G.; Cavaliere, C.; Riccioli, A.; Palchetti, S.; Lagana, A. *Langmuir* **2013**, *29*, 6485−6494.
(79) Caracciolo, G. *Bioinsp. Biomim. Nanobiomater.* **2012**, *2 BBNI*, 54−57.
(80) Caracciolo, G.; Pozzi, D.; Capriotti, A. L.; Cavaliere, C.; Lagana, A. *J. Nanopart. Res.* **2013**, *15*, 1498.
(81) Lesniak, A.; Salvati, A.; Santos-Martinez, M. J.; Radomski, M. W.; Dawson, K. A.; Aberg, C. *J. Am. Chem. Soc.* **2013**, *135*, 1438−1444.